chemosensors

MDPI

Review

Recent Progress with Bismuth Sulfide for Room-Temperature Gas Sensing

Renping Ma [1], Haoxin Lei [2], Mingyang Han [2] and Juanyuan Hao [2,*]

[1] Beijing Vocational College of Labour and Social Security, Beijing 100029, China; rpma@bvclss.edu.cn
[2] School of Materials Science and Engineering, Harbin Institute of Technology, Harbin 150001, China; 24s009009@stu.hit.edu.cn (H.L.); 2021112208@stu.hit.edu.cn (M.H.)
* Correspondence: jyhao@hit.edu.cn

Abstract: Monitoring hazardous gases is increasingly critical for environmental protection and human health. As a novel class of two-dimensional nanomaterials, layered metal chalcogenides have attracted substantial research attention in recent years. This is attributed to their unique physical and chemical characteristics, which endow them with remarkable potential for applications in gas sensing. In particular, bismuth sulfide (Bi_2S_3) has been extensively studied recently due to its cost-effectiveness, abundance, and eco-friendliness, aligning with the requirements of advanced sensing platforms. This article systematically summarizes recent advancements in gas sensors based on Bi_2S_3. Initially, the structural and functional properties of Bi_2S_3 are outlined, emphasizing its potential in detecting toxic gases. Subsequently, innovative methodologies aimed at enhancing room-temperature sensing efficiency are critically analyzed. The discussion concludes by addressing existing limitations and proposing future research directions to optimize Bi_2S_3 for practical applications. This review aims to systematically examine the design and optimization of next-generation gas detection nanomaterials, offering fundamental understanding of their performance enhancement mechanisms and exploring their potential implementation across multiple technological platforms.

Keywords: bismuth sulfide; gas sensors; innovative approaches; room-temperature sensing

check for updates

Received: 18 February 2025
Revised: 23 March 2025
Accepted: 27 March 2025
Published: 1 April 2025

Citation: Ma, R.; Lei, H.; Han, M.; Hao, J. Recent Progress with Bismuth Sulfide for Room-Temperature Gas Sensing. *Chemosensors* **2025**, *13*, 120. https://doi.org/10.3390/chemosensors13040120

Copyright: © 2025 by the authors. Licensee MDPI, Basel, Switzerland. This article is an open access article distributed under the terms and conditions of the Creative Commons Attribution (CC BY) license (https://creativecommons.org/licenses/by/4.0/).

1. Introduction

Gas sensors, designed for the detection of noxious and perilous gases, have been utilized in extensive applications across a wide range of domains, including agricultural and industrial manufacturing processes, food safety, and medical diagnosis procedures [1–3]. In the context of atmospheric surveillance, these gas sensors can quantify concentrations of nitrogen dioxide (NO_2) [4–9], hydrogen sulfide (H_2S) [10,11], and volatile organic compounds (VOCs) [12], thereby ensuring that environmental conditions remain conducive to human health and productivity [13–15]. In the context of hazard detection, gas sensors are of vital significance in the monitoring of combustible and explosive gases during industrial operations, thus mitigating the risk of injuries resulting from gas leaks [16]. Additionally, in the realm of medical diagnostics, non-invasive gas-sensing apparatuses are employed for the analysis of exhaled gases, which can indicate various pathological and metabolic states [17]. Studies have shown that the detection of acetone, ammonia (NH_3), and H_2S in breath samples can facilitate the preliminary diagnosis of conditions such as diabetes, kidney disease, and oral infections, respectively [18].

Currently, gas sensors demonstrate significant potential in applications such as intelligent home devices, advanced medical technology, and wearable devices [19,20]. Owing

to the increase in the Internet of Things (IoT), the essential necessities for advanced gas sensor development predominantly encompass cost-effectiveness and minimal energy consumption characteristics, and straightforward operational conditions [20,21]. Gas-sensing devices can be systematically classified according to their operational mechanisms, encompassing five primary categories: electrochemical detection systems, resistance-based chemical sensors (chemoresistive sensors), photonic measurement platforms, acoustic wave transduction devices, and catalytic oxidation detectors [22]. Among these, chemoresistive gas sensors are particularly favored for their affordability, ease of fabrication, and compatibility with integrated circuits [14]. However, traditional gas detection systems utilizing metal oxide semiconductor materials often necessitate elevated operational temperatures for optimal performance (ranging from 200 to 600 °C), which undermines their advantages for low-power integrated applications [12,23]. As a result, an increasing tendency is emerging regarding the development of novel sensing materials aimed at producing gas sensors that function effectively at room temperature.

Inspired by advancements in graphene research, there has been a marked increase in scientific interest surrounding two-dimensional (2D) materials, including layered metal chalcogenides (LMCs) [24], phosphorene [25], and MXenes [26,27]. Phosphorene, a monolayer of black phosphorus, exhibits exceptional carrier mobility and tunable bandgaps, making it promising for optoelectronic and sensing applications [25]. However, its chemical instability under ambient conditions due to rapid oxidation and moisture sensitivity severely limits its practical utility in gas sensors [28]. Similarly, MXenes, a family of transition metal carbides/nitrides, demonstrate high electrical conductivity and surface functionality [26]. Despite these advantages, their synthesis often requires hazardous etching agents (e.g., HF), and their irreversible adsorption behavior toward analytes complicates recovery performance in sensing applications [26]. Within this category, LMCs have gained significant attention as potential materials for gas detection systems due to their exceptional physicochemical properties, including remarkably high surface-to-volume ratios, superior charge transport capabilities, and enhanced surface chemical activity [29], rendering them more viable for real-world gas-sensing devices. The crystal structures of 2D LMCs are mainly stacked in the forms MX_2, MX, or M_2X_3, where M is a metallic element in the transition groups IVB-VIB (e.g., Mo, W, V, Nb, Zr, and Ta) or the main group IIIA-VA (e.g., Ga, In, Sn, Sb, and Bi), and X is a chalcogenide element (S, Se, or Te) [30,31]. The structural configuration of LMCs exhibits a distinctive anisotropic bonding arrangement, featuring robust covalent bonding within individual layers while demonstrating weak interlayer cohesion mediated by van der Waals forces. This architecture provides a substantial specific surface area, enhancing the adsorption kinetics and molecular diffusion dynamics of gaseous species [32]. Additionally, their superior electrical conductivity facilitates gas-sensing capabilities at low or room temperatures [33,34]. In comparison with graphene, phosphorene, and MXenes, LMCs exhibit remarkable sensitivity and selectivity in gas detection, enabling effective monitoring at parts per million or even parts per billion concentrations [35].

Among the family of LMCs, bismuth sulfide (Bi_2S_3) has garnered significant attention due to its abundance, non-toxicity, ease of surface modification, and low levels of heavy metals [36,37]. Bi_2S_3, a semiconductor material characterized by its narrow and adjustable bandgap ranging from 1.3 to 1.7 eV [38,39], exhibits exceptional performance in various applications, including optoelectronic apparatuses, electrocatalytic reduction processes, photocatalytic generation reactions, and especially gas-sensing applications [40–45], attributed to its unique structural characteristics.

However, pristine Bi_2S_3 is ineffective at room temperature due to its low inherent conductivity, leading to substantial energy consumption and complex equipment require-

ments, thus limiting its widespread adoption in state-of-the-art sensing platforms. Recently, significant research endeavors have been focused on enhancing the gas detection capabilities of Bi_2S_3 through the implementation of diverse material engineering approaches, including morphological design, defect engineering, heterostructure construction, and light irradiation.

This review provides an overview of established experimental and theoretical approaches related to Bi_2S_3-based gas-sensing materials. While previous reviews have covered preparation methods, performance evaluation parameters, and fundamental working principles of LMCs, this review comprehensively examines contemporary advancements in material engineering strategies specifically designed to enhance the ambient temperature gas detection performance of Bi_2S_3 nanostructures toward various toxic and hazardous gaseous compounds. Additionally, the primary challenges and prospects associated with Bi_2S_3-based gas sensors are outlined. It is anticipated that this article will contribute foundational insights to address the limitations of Bi_2S_3 and facilitate its broader application in the field.

2. Bi_2S_3: Rising Material for Gas-Sensing Applications

Bi_2S_3, as a newly-emerged constituent of LMCs, has attracted extensive attention due to its relatively low toxicity and eco-friendly characteristics. The crystal structure exerts a substantial influence on determining both the synthesis route and the characteristics of a material. Bi_2S_3 crystallizes in an orthorhombic structure, belonging to the space group Pbnm (62), with lattice constants of a = 1.114 nm, b = 1.130 nm, and c = 0.3981 nm [42,46]. Unlike typical van der Waals materials that possess a single distribution direction of van der Waals force, the crystal atoms of Bi_2S_3 are covalently bonded in just one direction, thereby forming long chains that are parallel to one another (Figure 1). Meanwhile, the adjacent two chains are joined via van der Waals forces along two separate directions [47].

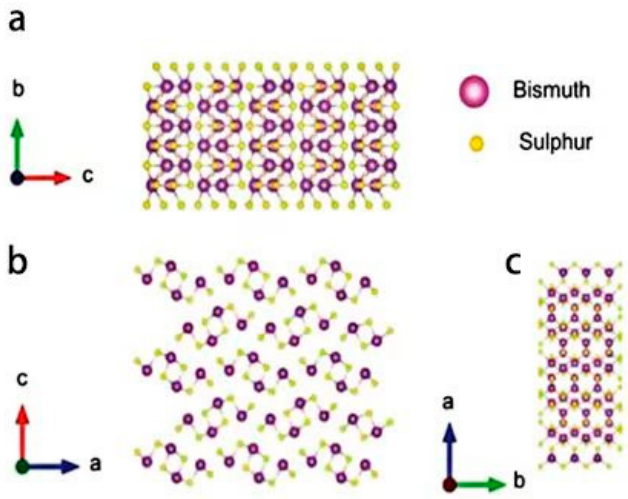

Figure 1. The crystal structure of Bi_2S_3 viewed from three axes: (**a**) b-c planes, (**b**) a-c planes, (**c**) a-b planes. Reproduced with permission from [48].

2.1. Gas Sensors Constructed with Pristine Bi_2S_3

A room-temperature H_2 sensor utilizing individual Bi_2S_3 nanowires was developed by Yao et al. [49]. This research represented a notable milestone in the field of Bi_2S_3-based gas sensing, achieving a detection sensitivity of 22% at a 10 ppm H_2 concentration at room temperature. This pioneering work established a foundation for elucidating the intrinsic sensing characteristics of Bi_2S_3 and paved the way for subsequent explorations into its potential in gas-sensing applications. Yang et al. [50] synthesized high-quality Bi_2S_3

single-crystalline nanowires, which demonstrated superior gas-sensing properties, especially for ethanol, outperforming conventional powders in terms of elevated response, more rapid response and recovery intervals, and favorable selectivity. The experimental results demonstrate that Bi_2S_3 nanowire-based architectures exhibit promising characteristics as advanced sensing materials for ethanol detection at ambient temperatures, suggesting their potential utilization in diverse technological applications requiring gas-monitoring capabilities.

Kan et al. [51] made contributions to the development of Bi_2S_3-based gas sensors. The sensors fabricated from Bi_2S_3 nanobelts treated with $Pb(NO_3)_2$ demonstrated enhanced responsiveness and recovery at ambient temperature, achieving a response value of 58.8 when exposed to 5 ppm of NO_2 (Figure 2). The incorporation of $Pb(NO_3)_2$ during ligand exchange eliminates insulating long-chain organic ligands (e.g., OLA and PVP) from Bi_2S_3 nanobelts, enabling the formation of a porous network. This process enhances gas adsorption and charge transfer by reducing surface insulation and optimizing interfacial interactions. The uniform Pb^{2+} distribution on nanobelt surfaces further modifies surface chemistry, contributing to structural refinement. The resulting interconnected nanobelt bundles exhibit a high specific surface area (13.59 m^2/g) and facilitate rapid gas diffusion. These structural advantages—enhanced porosity, efficient gas accessibility, and improved charge dynamics—collectively enhance gas-sensing performance, establishing Bi_2S_3 nanobelts as a promising material for low-power, cost-effective sensors. It is worth highlighting that the presence of adsorbed OH^- on the surface played a role in augmenting the sensors' sensitivity to NO_2. The ambient temperature response characteristics of Bi_2S_3 nanobelts, coupled with their outstanding solution process characteristics, render them highly promising in the development of economical gas sensors that consume less power.

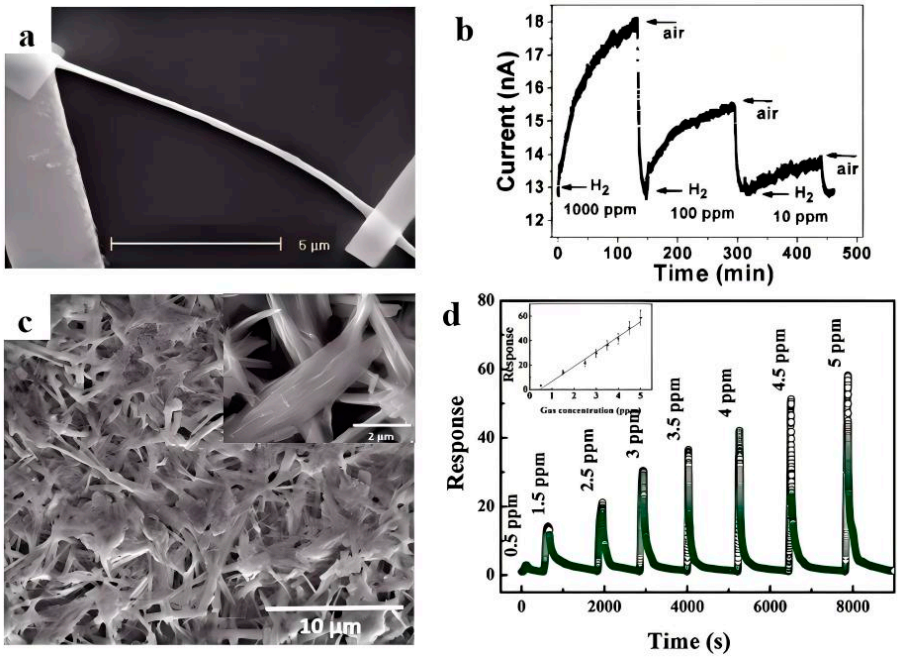

Figure 2. Structural and gas-sensing characterization of Bi_2S_3 nanowires and nanobelts. (**a**) SEM image of an individual Bi_2S_3 nanowire connected to Pt electrodes. (**b**) Hydrogen sensing response of Bi_2S_3 nanowires at 0.5 V bias under 10–1000 ppm H_2 in N_2, showing a sensitivity of 22% at 10 ppm. Reproduced with permission from [49]. (**c**) SEM image of Bi_2S_3 nanobelt film showing a porous network morphology (inset shows the corresponding high-magnification SEM image). (**d**) Sensing response of $Pb(NO_3)_2$-treated Bi_2S_3 nanobelts at room temperature under 0.5–5 ppm NO_2, demonstrating a response value of 58.8 at 5 ppm. Reproduced with permission from [51].

Feng et al. [52] explored Bi_2S_3's gas-sensing mechanisms using first-principles calculations. Their analysis covered adsorption, electronic properties, and gas diffusion on Bi_2S_3. Results highlighted Bi_2S_3's strong NO_2 selectivity, with high adsorption energy (−0.88 eV vs. −0.14 eV for CH_4), reduced bandgap (ΔG = 1.42 eV), and low NO_2 diffusion (9.09×10^{-4} cm^2/s). Experimental studies [53] confirmed these findings: solvothermal Bi_2S_3 nanobelts achieved 17 ppb NO_2 detection at room temperature, outperformed NH_3/CO selectivity, and showed humidity-enhanced sensitivity (−1.01 eV adsorption energy). Theoretical bandgap narrowing matched experimental conductivity improvements. Low NO_2 diffusion ensured stable adsorption, minimizing desorption. This computational–experimental synergy validates Bi_2S_3 as a high-performance NO_2 sensor.

Despite the performance in gas sensing achieved with Bi_2S_3, the burgeoning field of pristine Bi_2S_3 still encounters several challenges. Pure Bi_2S_3 has some drawbacks as a gas-sensing material. Its high room-temperature resistance and low response value make signal acquisition difficult. The long recovery time of pure Bi_2S_3-based sensors also limits their practical application. Moreover, the presence of long-chain surfactants on the surface of solution-processed Bi_2S_3 nanobelts reduces gas molecule accessibility and inhibits carrier transport, resulting in poor gas-sensing performance. Additionally, the recovery time of pure Bi_2S_3-based sensors is relatively long, up to 106 s even after $Pb(NO_3)_2$ treatment, which is not ideal for real-time gas detection applications [51].

For instance, pure Bi_2S_3 as a gas sensor exhibits inferior recovery performance (prolonged recovery time of approximately 400 s upon exposure to 1 ppm NO_2 [51]) and limited sensitivity to gases like NO_2 at room temperature due to its intrinsic poor conductivity [54]. This slow recovery behavior means that the sensor requires about 400 s to return to its baseline state after exposure to the target gas, which fundamentally hinders its application in real-time monitoring systems.

Furthermore, previous studies have demonstrated that pristine Bi_2S_3-based gas sensors typically exhibit a relatively high limit of detection (LoD) at room temperature, making it difficult to detect trace amounts of gases, which is crucial for early warning systems and precise environmental monitoring [55]. For example, Yao et al. reported a Bi_2S_3 nanowire-based H_2 sensor with an LoD of 10 ppm [49], while Yang et al. developed Bi_2S_3 nanowires for ethanol sensing, achieving a detectable concentration as low as 10 ppm [50]. However, unmodified Bi_2S_3 remains insufficient for trace-level NO_2 detection (e.g., parts-per-billion, ppb), primarily due to its limited surface reactivity and adsorption capacity. Even with surface modification (e.g., $Pb(NO_3)_2$ treatment), the LoD of NO_2 detection was only reduced to 500 ppb [51], which still fails to meet practical requirements for environmental monitoring. To address this limitation, strategies have been engineered to amplify sensing performance. Notably, hierarchical Bi_2S_3 architectures synthesized by Yang et al. [56] achieved an ultralow LoD of 50 ppb for NO_2, underscoring the critical role of morphology optimization in improving gas adsorption kinetics and charge transfer efficiency.

Additionally, while Bi_2S_3 shows good selectivity towards NO_2 in the presence of humidity [52], its overall performance is still not sufficient for reliable NO_2 sensing under ambient conditions. The study was mainly based on first-principles calculations, which are theoretical in nature. In practical applications, the morphology and size of Bi_2S_3 nanomaterials play crucial roles, which can influence the adsorption and diffusion of NO_2. Additionally, other factors such as surface defects and temperature fluctuations, which are common in real-world materials, can impact the sensing performance. Although Bi_2S_3 shows potential for selectively detecting NO_2 in humid environments, more research is needed to address these issues and improve its overall performance for reliable sensing under ambient conditions. These limitations highlight the need for modifications or the development of composite materials to improve the gas-sensing

capabilities of Bi_2S_3. To exploit the gas-sensing application of Bi_2S_3 at room temperature, specific structural modifications through functionalization strategies are essential to enhance its inherent properties.

2.2. Strategies for Enhancing Room-Temperature Sensing Performance

2.2.1. Morphological Design

Control over the morphology of materials is a highly efficacious strategy for modulating their properties, frequently employed in the synthesis of various compounds. By altering the synthesis methods or the precursors used, the morphology of materials can be readily manipulated. The characteristics of the configuration and architecture of gas-sensing materials are pivotal in the enhancement of their sensing performance, because these properties are contingent upon the dynamics of diffusion and the adsorption/desorption mechanisms involving the substances and the analyzed gases. Scientific investigations have focused on the optimization of morphological structures of Bi_2S_3, enhancing active sites and improving gas adsorption capabilities.

The synthesis of low-dimensional Bi_2S_3 nanostructures, such as nanowires [50], nanobelts [42,53], nanorods [57], and nanosheets [48], aims to enhance gas-sensing capabilities. However, the propensity of low-dimensional nanomaterials to undergo stacking and aggregation phenomena significantly compromises their functional effectiveness by reducing accessible active sites for gas adsorption, while simultaneously impeding molecular diffusion and adsorption-desorption kinetics, ultimately leading to the degradation of their inherent sensing capabilities [56,58]. Constructing hierarchical nanostructures offers a viable strategy to alleviate restacking and increase the active surface area, which enriches the sensing active sites and facilitates the diffusion and adsorption/desorption of gases on the nanomaterial surface [56]. In this regard, hierarchically structured Bi_2S_3 nanomaterials, characterized by their unique architecture and large surface area, emerge as highly promising candidates for sensing applications. As a result, extensive scientific investigations [39,56,59–62] have been focused on developing architecturally controlled Bi_2S_3 nanoarchitectures with enhanced surface-to-volume ratios through advanced synthesis methodologies.

Li et al. [62] pioneered the use of hydrothermal synthesis for creating hierarchical Bi_2S_3 nanostructures, showcasing their applicability in gas sensing, specifically focusing on methanol detection, as shown in Figure 3a,b. This work laid the groundwork for subsequent research into the gas-sensing capabilities of these complex architectures. The diversity in Bi_2S_3 nanomaterial morphologies, such as flower-like [44] and urchin-like [63], has been achieved through various synthesis techniques, aiming to augment their functional attributes. Notably, Fu and colleagues [61] prepared a 3D Bi_2S_3 nanowire network for NH_3 sensing at room temperature which underscored the advantage of large surface areas in enhancing sensing properties, as shown in Figure 3c–e. This research contributes to the understanding that morphological design of Bi_2S_3 can effectively amplify the sensing capabilities of low-dimensional materials, offering a pathway for optimizing nanostructures in gas-sensing applications.

Yang et al. [56] synthesized one-dimensional nanorods featuring self-assembled hierarchical Bi_2S_3 nanostructures synthesized through a straightforward hydrothermal method (Figure 4a). By constructing hierarchical nanostructures, abundant sensing active sites can be provided and monitoring of gas diffusion and adsorption/desorption on nanomaterial surfaces can be promoted. The gas-sensing material based on Bi_2S_3 nanostructures for NO_2 detection can work at room temperature. The hierarchical Bi_2S_3 nanostructures, composed of nanorods, exhibited exceptional NO_2 sensing behavior, exhibiting a large response value and quick response/recovery intervals (Figure 4b). The sensor's low limit of detection and

excellent selectivity, along with its humidity tolerance (Figure 4c–e), were attributed to the rich active sensing surface and expedited diffusion as well as the processes of adsorption and desorption occurring between NO_2 molecules and Bi_2S_3 materials.

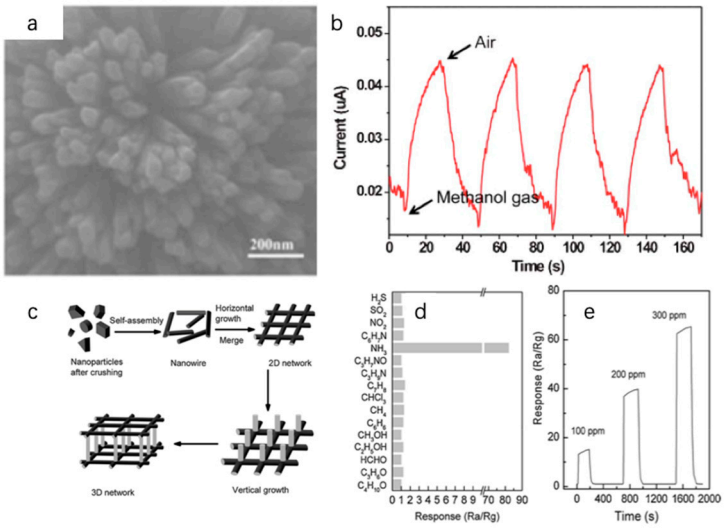

Figure 3. (**a**) SEM image of hierarchical Bi_2S_3 nanostructures. (**b**) Temporal variation of the current in the gas sensor based on hierarchical Bi_2S_3 nanostructures under a 0.5 V bias [62]. (**c**) Proposed self-assembly mechanism of Bi_2S_3 nanowires and their network. Response features of the 3D Bi_2S_3 nanowire networks sensor at 30 °C. (**d**) Responses to 360 ppm of different gases at 5 V. (**e**) Response transients for NH_3 at 5 V. Reproduced with permission from [61].

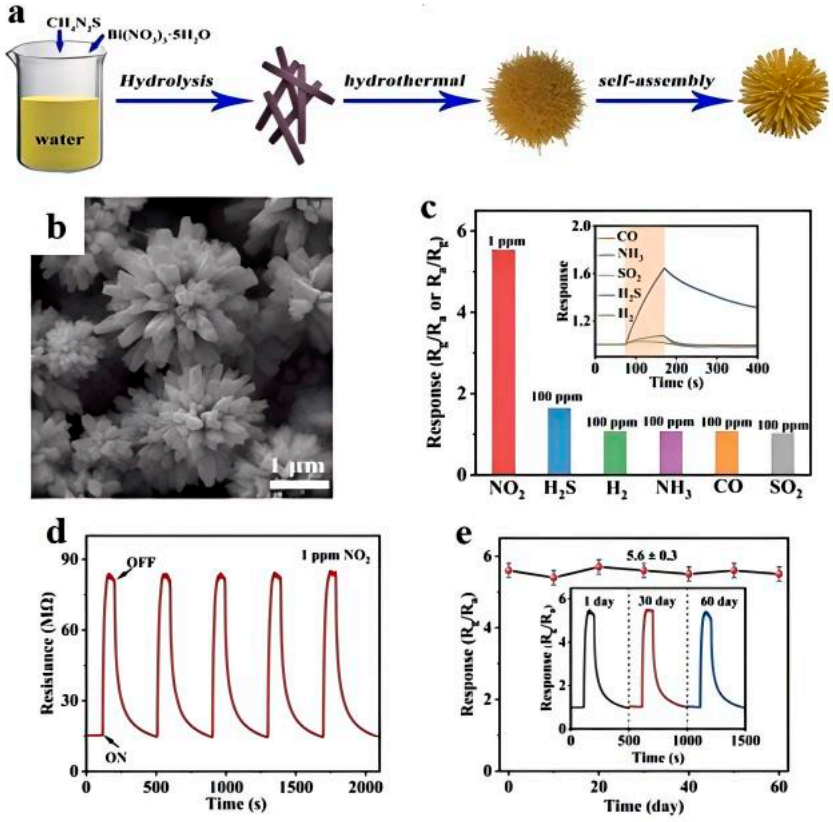

Figure 4. (**a**) Schematic illustration of the formation process, (**b**) SEM image of hierarchical Bi_2S_3 nanomaterials. The RT NO_2 sensing properties test of the samples: (**c**) Selectivity measurement toward interfering gases. (**d**) Baseline resistance and sensitivity to 1 ppm NO_2 under different humidity environments. (**e**) Long-term stability. Reproduced with permission from [56].

The fabrication of hierarchical structures emerges as an optimal approach to mitigate the aggregation of low-dimensional nanomaterials, thereby enhancing their gas-sensing capabilities. Such structures not only expand the active surface area available for interaction with target gases but also expedite the processes of adsorption, diffusion, and desorption. In the case of Bi_2S_3, various hierarchical nanostructures, such as urchin-like microspheres (composed of radially aligned nanorods) [64], 3D nanowire networks (interconnected porous frameworks) [61], flower-like architectures (self-assembled from nanoplates or nanorods) [44,65], and sheaf-like bundles (aligned nanorod aggregates) [66], have been successfully synthesized. These diverse forms of Bi_2S_3 nanostructures highlight the versatility in fabrication methods and underscore the significance of developing appropriate hierarchical configurations to enhance gas sensor sensitivity. For instance, urchin-like structures provide a high surface-to-volume ratio for efficient gas adsorption, while 3D networks facilitate rapid gas diffusion and electron transport, collectively improving sensing performance.

2.2.2. Defect Engineering

Defect engineering has emerged as a potent strategy to enhance the sensing performance of gas sensors, particularly those based on 2D metal sulfides. This approach involves regulating the kinetics of charge transport and introducing additional active sites to bolster the overall sensing capabilities of the materials. Considerable efforts have been directed towards engineering defects in Bi_2S_3 nanomaterials, leveraging their inherent properties to improve sensing performance.

Bi_2S_3 nanomaterials are particularly amenable to the formation of sulfur vacancies due to their low defect formation energy, which positions them as ideal candidates for defect engineering [57,67]. The incorporation of defects into Bi_2S_3 has been employed to enhance its photocatalysis, photothermal therapy, and photovoltaic applications, demonstrating the versatility of these materials in various fields [57,67,68]. The incorporation of defects into Bi_2S_3 has been extensively studied for enhancing its gas-sensing performance, particularly for room-temperature NO_2 detection. Unlike applications in photocatalysis or photovoltaics, where defects primarily improve charge carrier separation or light absorption, sulfur vacancies in Bi_2S_3 significantly amplify surface reactivity and electron depletion layer modulation, directly boosting gas adsorption and charge transfer kinetics [63,69]. In a recent study, Chen et al. [69] demonstrated a high-efficiency sensor motivated by neuronal conduction mechanisms, which led to significant advancements achieved in the sensitivity and selectivity features of gas-sensing materials. The strategic incorporation of sulfur vacancy defects through Au quantum dot modification resulted in enhanced sensor performance, demonstrating rapid response characteristics, exceptional sensitivity with ultra-low detection thresholds, and remarkable mechanical durability under repeated deformation cycles. These findings provide compelling evidence for the critical function of sulfur vacancies in achieving highly selective and ultrasensitive NO_2 detection capabilities.

In a study by Yang et al. [63], urchin-like Bi_2S_3 nanostructures with an abundance of sulfur vacancies were fabricated via the hydrothermal method (Figure 5a), enabling the detection of NO_2 at the ppb level at room temperature. Gas sensors with an urchin-like morphology (Figure 5b–e) facilitate gas adsorption, diffusion, and desorption. These sensors demonstrate high sensitivity, rapid response and recovery times, and the ability to detect NO_2 at the ppb level at room temperature (Figure 5f–h). The results suggest that urchin-like Bi_2S_3 nanostructures, rich in sulfur vacancies, show significant potential for the evolution of sophisticated gas-sensing devices.

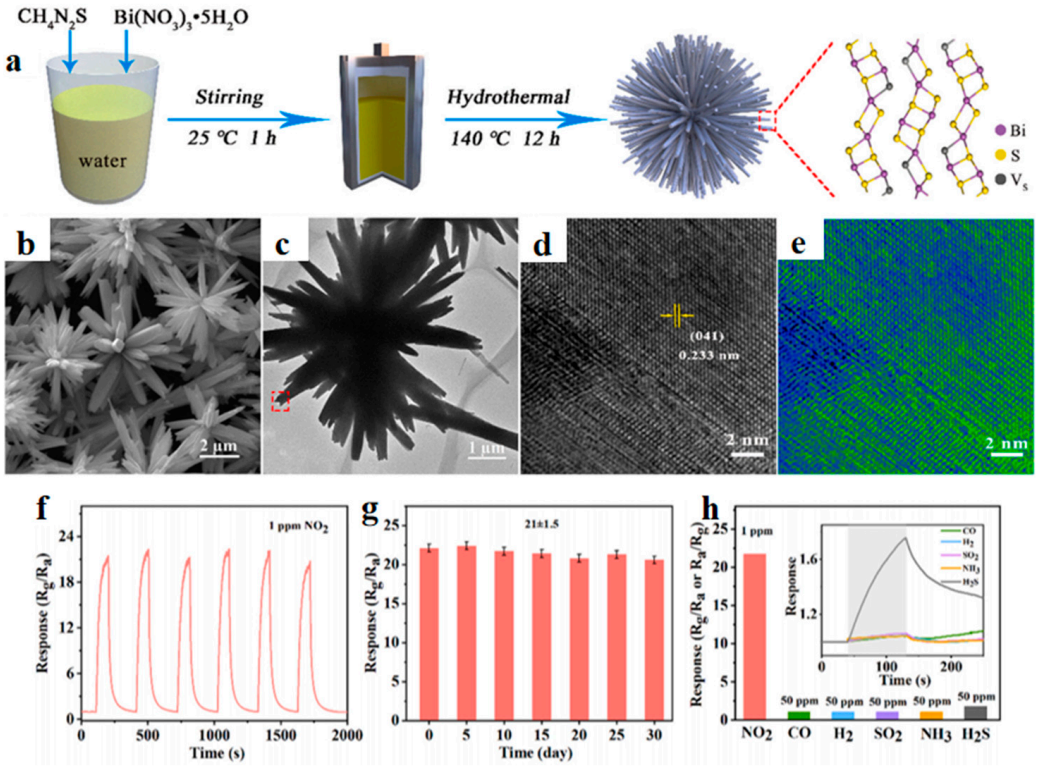

Figure 5. (**a**) Schematic representation of the preparation procedure for urchin-like Vs-Bi_2S_3. (**b**) SEM, (**c**) TEM, (**d**) HRTEM and (**e**) false-color images of the BS-4 sample. (**f**) Six consecutive sensing cycles for 1 ppm NO_2. (**g**) Long-term stability toward 1 ppm NO_2 for 30 days. (**h**) Selective response toward different gases. Reproduced with permission from [63].

Kan and colleagues [55] utilized a hot-injection synthesis approach to engineer Bi_2S_3 nanorod structures, which were subsequently used to create sensor devices via spin-coating onto Al_2O_3 ceramic substrates. These strategies enable the accurate regulation of both the aspect ratio of the nanorods and the concentration of sulfur vacancies. These modifications significantly enhanced electron transfer within the film and augmented the number of active sites on the Bi_2S_3 nanorods. This work reveals that a gas sensor constructed with Bi_2S_3 nanorods with Bi/S = 4:1 displays exceptional sensitivity to NO_2 at room temperature, accompanied by rapid response and recovery kinetics.

In conclusion, defect engineering in Bi_2S_3 gas sensors holds great promise for improving sensing performance. The strategic introduction of sulfur vacancies and the integration of heterostructures have been shown to significantly enhance the detection of NO_2. To elucidate the correlation between the defect density and gas-sensing performance, further investigations are indispensable, which could offer valuable insights for the design of innovative sensing materials. These advancements underscore the importance of defect engineering in the development of next-generation gas sensors with improved sensitivity, selectivity, and stability.

2.2.3. Heterostructures Construction

The fabrication of heterogeneous architectures has turned out to be a promising strategy for improving gas detection capabilities, primarily through facilitating effective charge carrier separation, modulating carrier concentration, and generating additional active sites at interfacial regions [29,70,71]. The integration of Bi_2S_3 with various materials to form heterojunction structures has emerged as a promising approach in enhancing gas-sensing capabilities, particularly for the detection of NO_2 and other gases [52,72]. This

section summarizes the recent advancements in Bi_2S_3 heterojunction-based gas sensors, highlighting their improved sensing performance and potential applications.

Chen et al. [73] developed a gas detection mechanism utilizing CuS quantum dot-decorated Bi_2S_3 nanosheet heterostructures, inspired by artificial neural networks, which achieved high-sensitivity NO_2 sensing. The incorporation of CuS quantum dots significantly improved NO_2 detection sensitivity, attributed to their high density of active sites and pronounced quantum confinement effects, while the Bi_2S_3 nanosheets served as an efficient charge transfer network channel. This neuron-like sensor showed a markedly improved response value, outstanding responsiveness, rapid recovery rate, a low theoretical detection threshold, and exceptional selectivity towards NO_2. The wearable device developed could visualize NO_2 detection through real-time signal changes. Chen et al. [73] investigated the synergistic NO_2-sensing mechanisms of CuS quantum dots (QDs) and Bi_2S_3 nanosheets (NSs) using density functional theory (DFT) and experimental validation. DFT calculations revealed that NO_2 preferentially adsorbs on CuS QDs via N-Cu bonding (binding energy: 2.25 eV), with significant charge transfer (3.371 e) confirmed by charge density difference analysis (Figure 6a,b). Bi_2S_3 NSs, while exhibiting minimal direct NO_2 adsorption, functioned as a high-mobility charge transport network. The CuS/Bi_2S_3 heterojunction formed a built-in electric field due to interfacial electron transfer, amplifying resistance changes during gas exposure (Figure 6c). Further analysis of the type-II band alignment (Bi_2S_3 CB: −4.37 eV; CuS: −4.79 eV) demonstrated band bending at the interface, creating electron-depleted Bi_2S_3 and hole-rich CuS layers. This alignment optimized charge separation and enabled ultrafast response (18 s) and high sensitivity (response: 3.4 to 10 ppm NO_2). The study highlights how DFT-guided heterojunction design overcomes the limitations of individual materials, achieving biomimetic NO_2 sensing at room temperature.

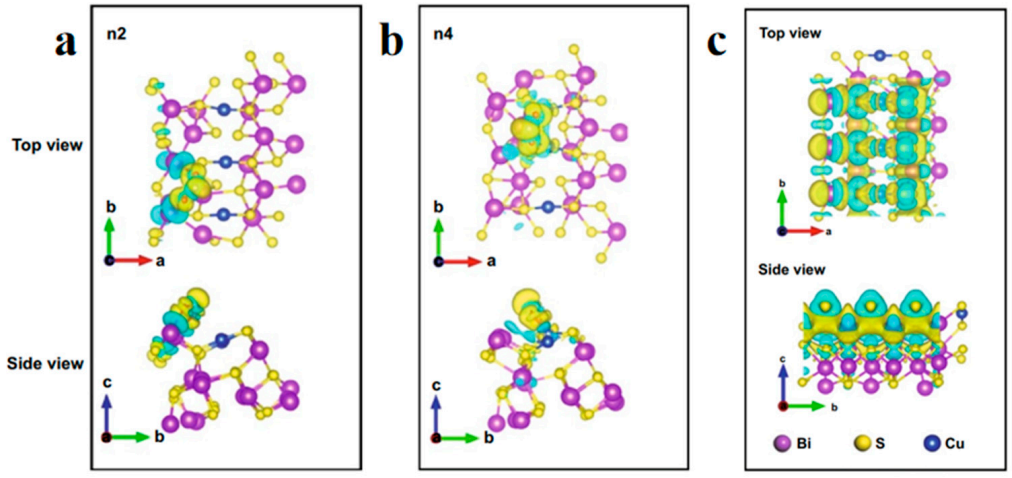

Figure 6. (**a**,**b**) Diagrams of charge density difference of NO_2 on CuS-Bi_2S_3 with n2 and n4 binding structure for side and top view, where the charge density isosurfaces of blue and yellow are 0.0015 and −0.0015 e $Å^{-3}$, respectively. (**c**) Charge distribution at the interface of CuS QDs and Bi_2S_3 NSs calculated by density functional theory. Reproduced with permission from [73].

Pei et al. [74] fabricated Bi_2S_3/Bi_2MoO_6 nanocomposites featuring a heterogeneous cookie-shaped structure. The research team also explored the gas-sensing characteristics of the Bi_2S_3/Bi_2MoO_6 nanocomposite in response to alcohol and n-hexane. The Bi_2S_3/Bi_2MoO_6 nanocomposite exhibited superior gas-sensing properties compared to pure Bi_2MoO_6, further enhancing its potential for application as a gas sensor. The Bi_2S_3/Bi_2MoO_6 nanocomposite forms a type-II heterojunction due to the alignment of their energy bands, which facilitates efficient charge separation. The heterojunction interface significantly amplifies gas-sensing performance through increased active sites and

catalytic activation. What is more, synergistic surface chemistry at the heterojunction accelerates redox reactions.

Zhao et al. [75] synthesized MoS_2-modified Bi_2S_3 heterojunctions which displayed ultrafast NO_2 response at 200 °C, underscoring the significance of extra active sites in the heterojunctions. Despite these improvements, there is a consensus that further enhancements in sensitivity, recovery, and ppb-level detection at room temperature are necessary. Expanding on this, the synthesis of Bi_2S_3/MoS_2 hybrid aerogels, featuring a distinctive parallel heterojunction structure with MoS_2 nanoflakes layered on Bi_2S_3 nanorods, was achieved by Liu et al. This particular Bi_2S_3/MoS_2-2 configuration demonstrated superior sensing capabilities when compared to sensors based solely on Bi_2S_3 or MoS_2 [40]. The enhanced performance of this composite sensor provides significant insights for the development and engineering of room-temperature sensors that leverage the properties of both Bi_2S_3 and MoS_2.

The integration of Bi_2S_3 with $Ti_3C_2T_x$ nanosheets yielded composite nanomaterials with enhanced gas-sensing properties. The $Ti_3C_3T_x$ MXene/Bi_2S_3 woven nanomesh structures, synthesized by a hydrothermal method, exhibited an excellent response and fast response/recovery at room temperature upon exposure to 1 ppm NO_2 [26]. The smart wearable wireless NO_2 monitoring system developed is capable of transmitting signals to be displayed in smartphone apps in real time, offering a new approach to improve the comprehensive performance of gas sensors and promote the application of composites in flexible gas sensors.

Lately, $Bi_2S_3/Ti_3C_2T_x$ nanomaterials were successfully synthesized and demonstrated enhanced responsiveness in real-time NH_3 monitoring as humidity levels rose [76]. Specifically, under 90% relative humidity, the response value increased to 1.32 times that under normal humidity conditions. This remarkable moisture resistance enables the sensor to maintain stability and performance in challenging environments.

The synthesis of hierarchical structures combined with heterojunction effects offers a prospective approach for enhancing the sensing performance. For instance, the integration of hierarchical nanoheterojunctions, such as those reported by Hao et al. [77] with SnS_2/SnO_2, has demonstrated ultrasensitive detection of NO_2 due to an increased number of active sites. For instance, Yang et al. [54] fabricated materials for room-temperature NO_2 detection with high sensitivity. These materials, consisting of Bi_2S_3 nanoflowers and reduced graphene oxide (rGO), were synthesized via an in situ hydrothermal approach (Figure 7a–d). The rGO/Bi_2S_3 sensor demonstrates a high response of 9.8 and a fast response time of 22 s when exposed to 1 ppm NO_2 at room temperature. Additionally, the sensor exhibits excellent humidity independence, selectivity, and stability (Figure 7e–g). The enhanced NO_2 detection performance primarily originates from synergistic heterointerface effects and hybrid structural advantages, which facilitate optimized charge transfer kinetics at the interface between NO_2 molecules and the rGO/Bi_2S_3 composite surface. This research provides valuable insights for enhancing the NO_2 sensing performance of metal chalcogenides.

Yang et al. [78] strategically integrated vacancy defect modulation with heterostructure engineering to develop BiOCl/Bi_2S_{3-x} heterojunctions with controlled sulfur vacancies, demonstrating enhanced NO_2 detection capabilities. The BiOCl/Bi_2S_{3-x} heterostructures featuring abundant S vacancies were fabricated through a straightforward one-step hydrothermal approach (Figure 8a–d). The optimized sensor, constructed on the S-vacancy-rich BiOCl/Bi_2S_{3-x} heterostructure, displayed a high response value (Rg/Ra = 29.1) to 1 ppm of NO_2 at room temperature, roughly 17-fold higher than that of pure Bi_2S_3. Furthermore, the developed sensor demonstrated superior performance metrics, featuring rapid response kinetics, ultra-low theoretical detection limits, excellent operational stability,

outstanding selectivity, and mechanical flexibility (Figure 8e–g). This investigation provides a strategic methodology for synergistic defect engineering and heterostructure design to achieve advanced room-temperature gas detection capabilities.

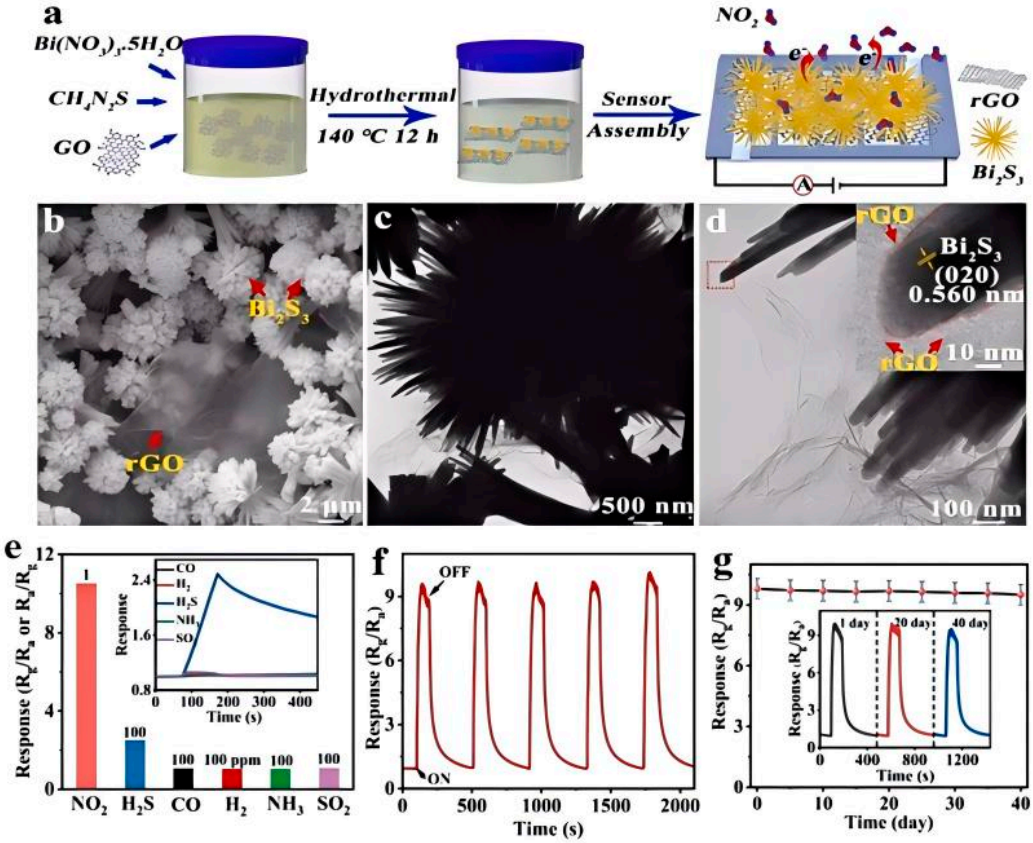

Figure 7. (**a**) Schematic representation of the synthesis of the rGO/Bi_2S_3 heterostructures. (**b**) SEM, (**c**) TEM, (**d**) HRTEM images. (**e**) Selectivity assessment against interfering gases. (**f**) Responsivity evaluation during six consecutive response–recovery cycles to 1 ppm NO_2. (**g**) Long-term stability examination upon exposure to 1 ppm NO_2. Reproduced with permission from [54].

Hu et al. [79] achieved the successful synthesis of high-quality Bi_2S_3/CuO heterostructures (Figure 9a–d). The Bi_2S_3/CuO-based sensor exhibited a response value of 31.2 to 1 ppm of H_2S, which was five-fold higher than that of pure Bi_2S_3. The enhanced detection capabilities primarily originate from synergistic heterojunction effects and increased surface chemisorption of oxygen at interfacial regions. Additionally, the sensor manifested a remarkably short response time, notable selectivity, dependable repeatability, outstanding moisture resistance, favorable long-term stability, and an exceedingly low detection limit of 25 ppb for H_2S (Figure 9e–g). This study emphasizes the viability of Bi_2S_3/CuO as an effective sensing material for H_2S gas detection at room temperature, providing valuable perspectives for the development of heterojunction sensors.

In conclusion, the development of Bi_2S_3 heterojunction structures has significantly advanced the field of gas sensing, offering a range of innovative solutions for improving sensor performance. These advancements not only enhance the detection capabilities for specific gases but also pave the way for the creation of smart, flexible, and reliable gas-sensing technologies.

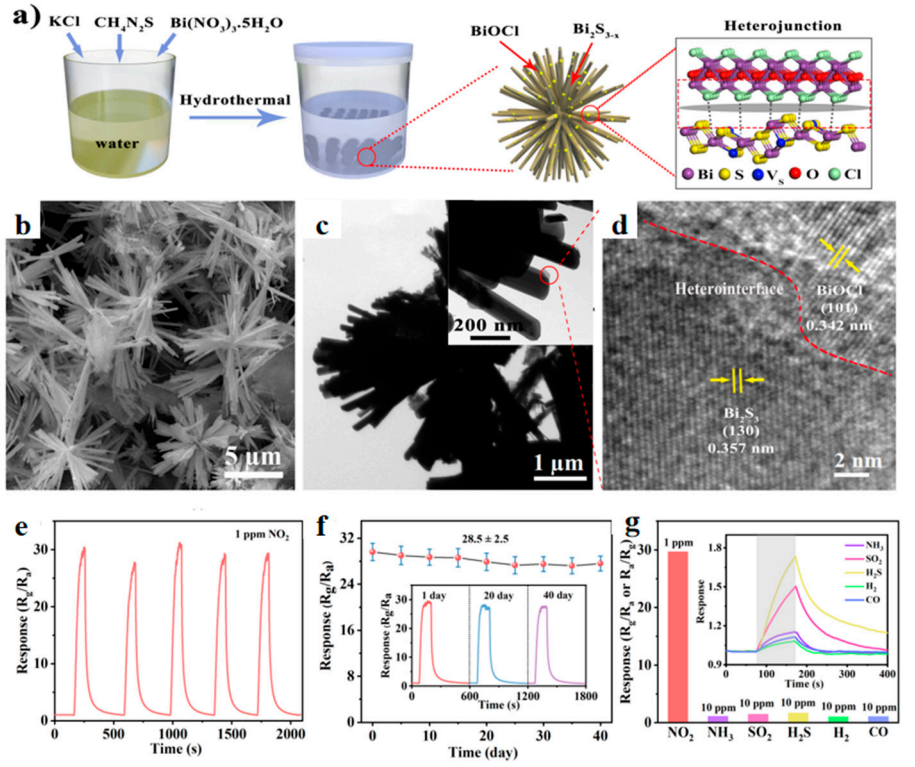

Figure 8. (**a**) Schematic representation of the synthesis process of BiOCl/ Bi_2S_{3-x} heterostructures, (**b**) SEM image, (**c**) TEM images, (**d**) HRTEM image. (**e**) Repeatability assessment over five consecutive cycles. (**f**) Long-term stability evaluation for 40 days against 1 ppm NO_2. (**g**) Selectivity test for NO_2, NH_3, SO_2, H_2S, H_2, and CO. Reproduced with permission from [78].

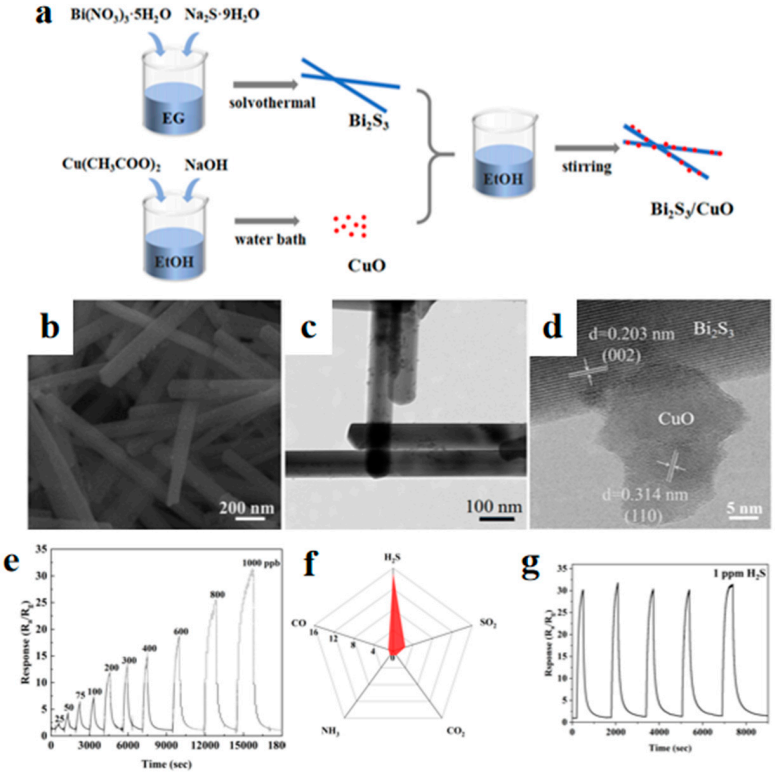

Figure 9. (**a**) Synthetic process, (**b**) SEM, (**c**) TEM and (**d**) HRTEM images of Bi_2S_3/CuO heterostructures. (**e**) Dynamic response–recovery curve of Bi_2S_3/CuO-2 to 25–1000 ppb H_2S. (**f**) Assessment of the selectivity of the Bi_2S_3/CuO-2 sensor for H_2S gas in comparison with other gases. (**g**) Repeatability test of Bi_2S_3/CuO-2 for 1 ppm H_2S with five continuous cycles. Reproduced with permission from [79].

2.2.4. Light Irradiation

Beyond optimizing the intrinsic structure of sensing materials, external auxiliary strategies have proven to be effective in enhancing sensing performance [80]. Among these, light-activated gas sensors have attracted substantial interest owing to their outstanding potential for gas sensing at room temperature [81]. Light activation enables the generation of energetic charge carriers, thereby modifying surface electronic characteristics and facilitating enhanced gas–solid interactions. Consequently, light irradiation serves as an effective strategy for simultaneously improving sensor response magnitude and accelerating reaction kinetics during both gas adsorption and desorption processes [82].

Wang et al. [41] presented a novel strategy for developing bifunctional gas sensors using Bi_2S_3/SnS_2 heterostructures, which exhibit enhanced sensitivity and selectivity for detecting NO_2 and H_2S at room temperature. The Bi_2S_3/SnS_2 heterostructures were fabricated via a two-step solvothermal approach. The Bi_2S_3/SnS_2 heterostructures possessed flower-like morphology, and the Bi_2S_3 nanoparticles were homogeneously adhered to the surface of hierarchical SnS_2 (Figure 10a–c). This work demonstrated that pristine SnS_2 can detect NO_2 solely under illumination owing to its low conductivity at room temperature. Bi_2S_3 showed weak responses to NO_2 and H_2S, with light having a minor modulating effect. In contrast, the Bi_2S_3/SnS_2 (BS-2) heterostructure exhibited ultrahigh sensitivity to NO_2 under light and high selectivity to H_2S in the dark (Figure 10d). The study demonstrates that the sensor's performance is significantly modulated by visible light, achieving ultrahigh response values of 14.0 (Rg/Ra) for 500 ppb NO_2 under light irradiation and 12.3 (Ra/Rg) for 500 ppb H_2S in the dark.

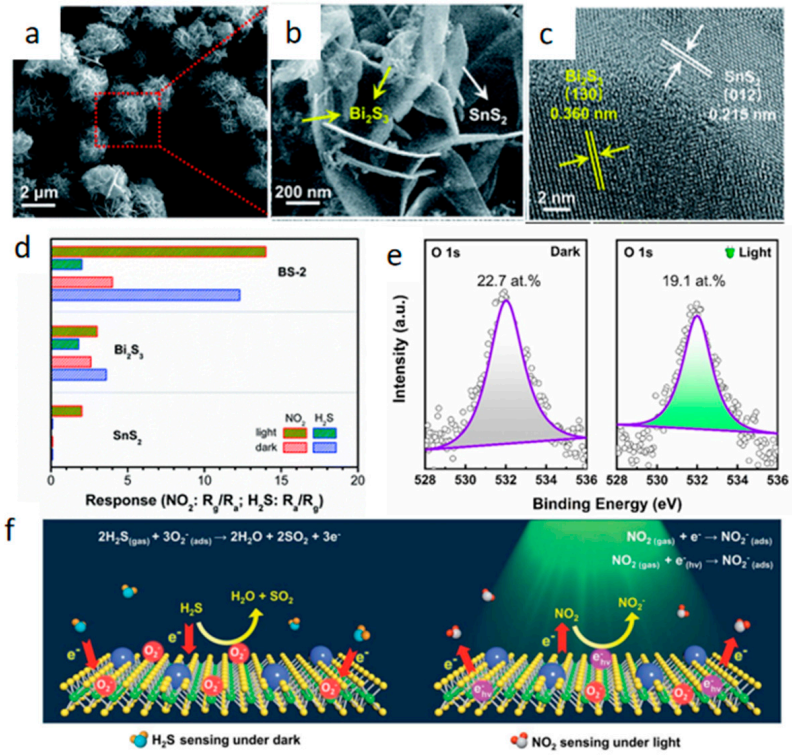

Figure 10. (**a**–**c**) SEM and HRTEM images of the synthetic process of the Bi_2S_3/SnS_2 heterostructures. (**d**) Summarized sensing responses of the SnS_2, Bi_2S_3, and BS-2 sensor to 500 ppb NO_2 and H_2S in the dark and under light illumination. (**e**) The in situ O 1s XPS spectra of Bi_2S_3/SnS_2 heterostructure in the dark and under 525 nm light illumination. (**f**) Schematic of the bifunctional H_2S and NO_2 sensing process of Bi_2S_3/SnS_2 heterostructures under dark and light conditions. Reproduced with permission from [41].

The bifunctional sensing mechanism of the Bi_2S_3/SnS_2 heterostructure originates from the synergy between heterojunction-induced charge modulation and photoactivation. The n-n heterojunction, formed due to the work function mismatch (Bi_2S_3: 4.65 eV; SnS_2: 5.05 eV), facilitates electron transfer from Bi_2S_3 to SnS_2, equilibrating Fermi levels and boosting SnS_2 conductivity. This interfacial charge redistribution creates depletion/accumulation layers, expanding reactive sites as reflected by the increased specific surface area (24.3 vs. 17.6 m^2/g for pure SnS_2). Visible-light irradiation generates electron–hole pairs that desorb pre-adsorbed oxygen (O_2^-), evidenced by in situ XPS revealing a decrease in surface oxygen from 22.7% to 19.1% (Figure 10e). The selectivity arises from distinct sensing models: H_2S detection follows an oxygen-mediated redox mechanism, while NO_2 sensing relies on physisorption-driven electron trapping. Light-activated oxygen desorption dynamically modulates active site availability (Figure 10f), achieving dual functionality: enhanced NO_2 response under illumination and optimized H_2S sensitivity in the dark.

The Bi_2S_3/SnS_2 sensor also demonstrates swift response–recovery kinetics, remarkable repeatability, and dependable stability towards ppb-level target gases. This work highlights the potential of visible light modulation in designing multifunctional gas sensors and suggests that Bi_2S_3/SnS_2 heterostructures could be promising material platforms for next-generation detection systems in IoT-enabled smart technologies.

Inspired by bifunctional gas sensors for detecting NO_2 and H_2S, researchers discovered that Bi_2S_3 can also be utilized for the detection of H_2S. In the process of H_2S sensing, a specific concentration of oxygen is beneficial [83]. In the dark, the existence of a greater amount of surface-adsorbed oxygen can lead to a more pronounced H_2S sensing response [41]. The Bi_2S_3/ZnS heterostructures displayed a substantial response to H_2S in the dark, approximately four-fold higher than that of pure Bi_2S_3 under indoor light [84]. Furthermore, the Bi_2S_3/ZnS-based sensor demonstrated exceptional operational characteristics, including superior gas selectivity, excellent reproducibility, remarkable long-term stability, and robust resistance to humidity variations (Figure 11a).

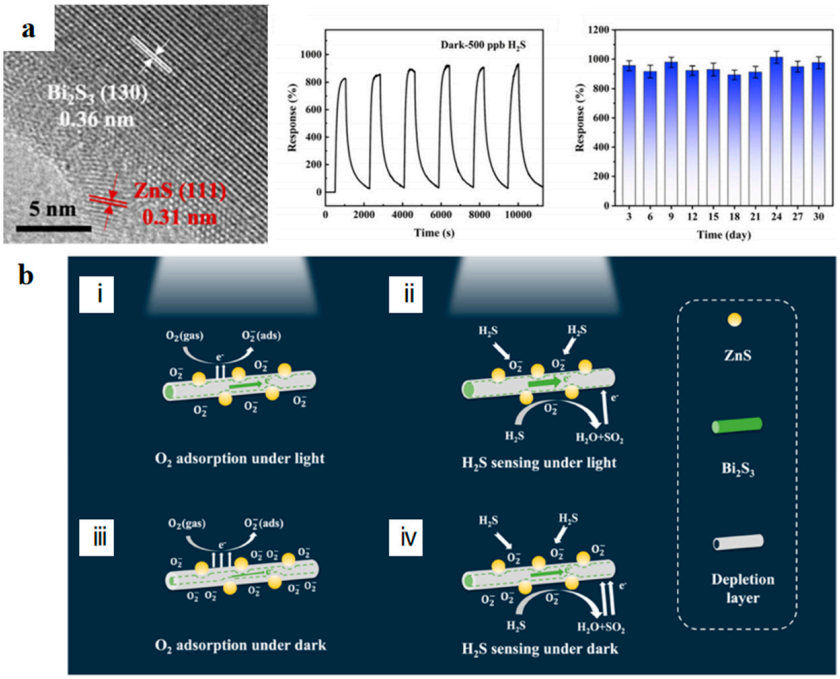

Figure 11. (**a**) HRTEM images of Bi_2S_3/ZnS heterostructures, repeatability and stability measurement of the Bi_2S_3/ZnS sensor to 500 ppb H_2S in the dark. (**b**) Schematic of the H_2S sensing process under (**i**,**ii**) light and (**iii**,**iv**) dark conditions for Bi_2S_3/ZnS heterostructures. Reproduced with permission from [84].

The sensing mechanism of Bi_2S_3/ZnS heterostructures toward H_2S is illustrated in Figure 11b, based on the oxygen adsorbate-mediated model. When exposed to air, these heterostructures adsorb oxygen to form O_2^-(ads), which reacts with H_2S, causing sensor resistance changes. The enhanced gas-sensing performance of Bi_2S_3/ZnS heterostructures in the dark is attributed to two main factors. First, the n-n heterojunction formed between ZnS nanoparticles and Bi_2S_3 nanowires improves the sensing response. Surface potential measurements show Bi_2S_3 and ZnS have work functions of 4.83 and 4.97 eV, respectively. Electron diffusion from Bi_2S_3 to ZnS increases the resistance of the heterostructures, aiding in effective electron–hole pair separation and enhancing sensor response. Under visible light, electron transfer forms a depletion layer at the Bi_2S_3 interface and an accumulation layer at the ZnS interface, providing more active sites for gas adsorption (Figure 11b i and ii). Consequently, Bi_2S_3/ZnS heterostructures exhibit an enhanced gas-sensing performance compared to pristine Bi_2S_3 and ZnS. Second, increased oxygen adsorption on the material surface in the dark boosts the sensor's response to H_2S. Under light, photo-excitation generates electron–hole pairs, with holes reacting with O_2^-(ads) to form oxygen molecules. Thus, as illustrated in Figure 11b (iii and iv), the depletion layer on the material surface becomes thicker, as well as the concentration of electrons being lower in the dark compared with that under visible light illumination. Based on the aforementioned reasons, the n-n heterostructure and light modulation contribute to the superior sensitivity and selectivity of Bi_2S_3/ZnS heterostructures toward H_2S.

Bi_2S_3/Sb_2S_3 heterostructures generate photoinduced oxygen anions under visible-light exposure, leading to an enhanced H_2S sensing ability [10]. The Bi_2S_3/Sb_2S_3 heterostructure sensor (Figure 12a) exhibited a notable rise in the sensing response to H_2S under indoor lighting compared to its performance in the dark. The enhanced H_2S sensing performance of the Bi_2S_3/Sb_2S_3 heterostructure under light irradiation results from the synergistic heterojunction and photoinduced effects (Figure 12b). The n-n heterojunction optimizes electronic properties, with electron transfer from Sb_2S_3 to Bi_2S_3 forming depletion and accumulation layers, providing additional gas adsorption sites and enhancing charge transfer. Under illumination, photoexcitation generates electron–hole pairs, whose separation is enhanced by the built-in electric field, increasing adsorbed oxygen ions that react more readily with H_2S. However, excessive light intensities can reduce sensitivity by decreasing O_2^- content. Overall, the combined heterojunction and photoinduced effects elevate O_2^- levels on the sensor surface, enabling sensitive H_2S detection under room-temperature illumination.

One-dimensional Bi2S3 nanorods are composited with 2D vanadium-based MXene nanosheets to construct Schottky heterojunctions as NO_2 room-temperature sensing materials [85]. Such a composite sensor demonstrates a substantial response (~190%) to 20 ppm of NO_2. Aided by UV illumination during the recovery process and the synergistic effect of the heterojunction, the composite sensor can fully recover to the baseline with a much shorter recovery time (103 s). Furthermore, the results demonstrate that the composite sensor achieves a reversible NO_2 detection of 0.25−40 ppm, as well as excellent stability and selectivity to NO_2.

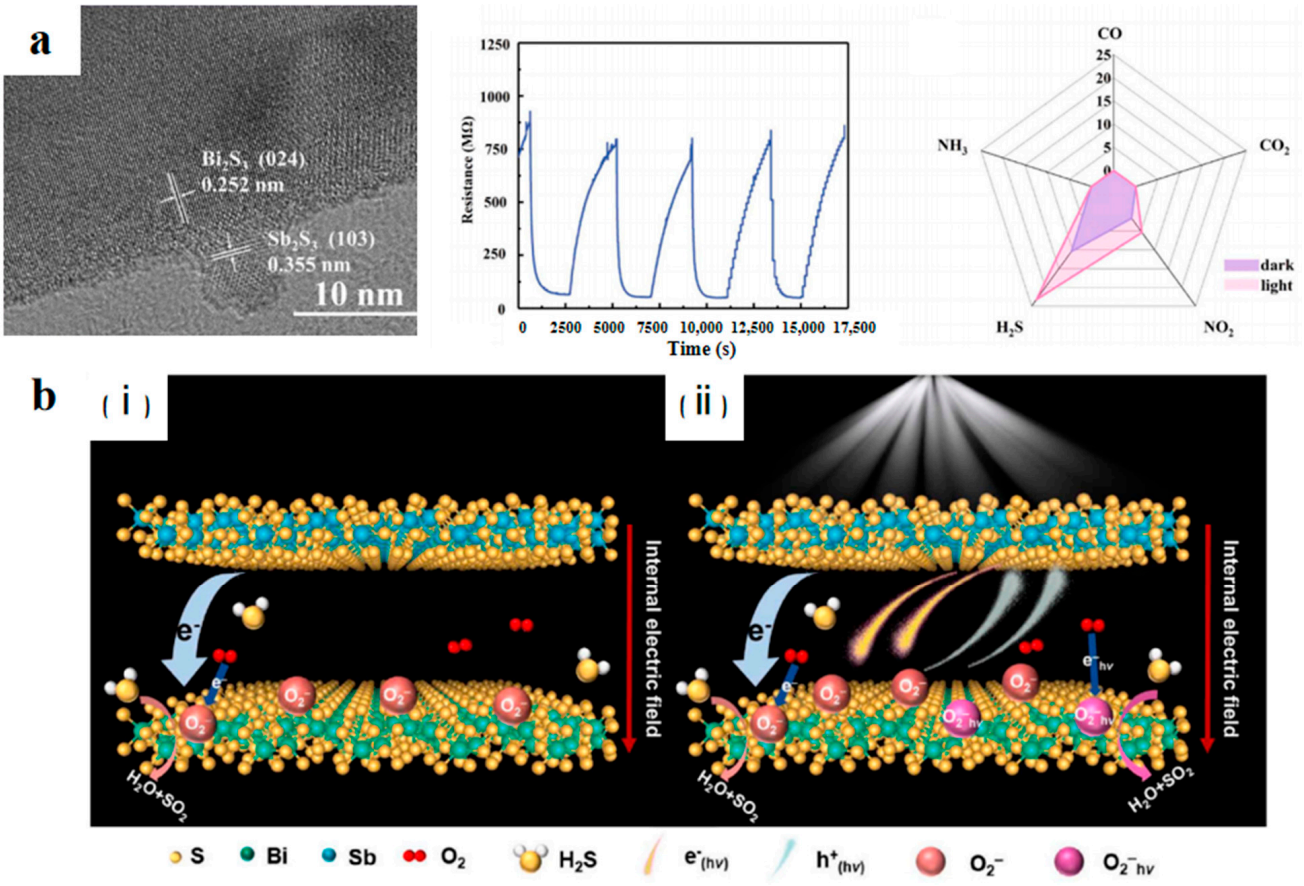

Figure 12. (**a**) HRTEM images, repeatability and selectivity measurement of the Bi_2S_3/Sb_2S_3 heterostructure. (**b**) Schematic of the H_2S sensing process under (**i**) dark and (**ii**) light conditions for Bi_2S_3/Sb_2S_3 heterostructures. Reproduced with permission from [10].

3. Conclusions and Outlook

The recent advances in Bi_2S_3-based gas sensing have demonstrated the potential of structural design and material engineering to significantly enhance sensor performance. Morphological design, defect engineering, heterostructure construction and light irradiation have all contributed to improvements in sensitivity, selectivity, response time, and stability.

A considerable portion of the reported Bi_2S_3-based gas sensors has been used for detecting NO_2, which suggests that Bi_2S_3-based gas sensors have a good response capability to NO_2. However, Bi_2S_3 exhibits good responsiveness to NO_2 and high selectivity towards H_2S. If the response ratio of Bi_2S_3-based gas sensors to NO_2 and H_2S under the same conditions is not significantly different, it would lead to poor selectivity of the Bi_2S_3-based gas sensors. This would prevent them from accurately determining whether the gas present in the environment is specifically NO_2 or H_2S, and also from conducting quantitative gas analysis. Consequently, this would render the sensor unsuitable for environments with complex gas mixtures, resulting in inferior sensor performance. Future research should focus on elucidating the factors that account for these differences in selectivity.

Investigations into the selectivity of Bi_2S_3 towards various gases can bolster its utility in practical applications. Enhancing the selectivity of Bi_2S_3-based gas sensors would facilitate the precise detection and quantification of specific gases within complex settings, a capability essential for environmental monitoring, industrial safety, and healthcare applications. Improved selectivity would mitigate the risk of false positives and enhance the reliability of gas detection, positioning Bi_2S_3 as a more valuable material in the realm of gas-sensing technologies.

Funding: This work was financially supported by the National Natural Science Foundation of China (No. 52272147).

Conflicts of Interest: The authors declare no conflict of interest.

References

1. Wang, H.; Lustig, W.P.; Li, J. Sensing and Capture of Toxic and Hazardous Gases and Vapors by Metal-Organic Frameworks. *Chem. Soc. Rev.* **2018**, *47*, 4729–4756. [CrossRef]
2. Zhang, H.; Xiao, J.; Chen, J.; Zhang, L.; Zhang, Y.; Pei, X.-L. Pd-modified $SmFeO_3$ with hollow tubular structure under light shows extremely high acetone gas sensitivity. *Rare Met.* **2022**, *42*, 545–557. [CrossRef]
3. Yao, L.; Zhao, Z.; Chen, C.; Shao, Z.; Wu, L. Fabrication of BI_2S_3/ZnO nanocomposites for TEA gas sensors operating at room temperature: Towards seafood freshness detection during storage. *Microchem. J.* **2024**, *207*, 112239.
4. Wang, Y.; Tang, C.; Su, M.; Ji, Y.; Xie, L.; Yang, Q.; Du, A.; Zhou, Y.; Yang, J. Highly sensitive, humidity-tolerant and flexible NO_2 sensors based on nanoplate Bi_2Se_3 film. *Chin. Chem. Lett.* **2023**, *34*, 107981. [CrossRef]
5. Wang, T.-T.; Xing, B.-S.; Guo, C.-Y.; Hao, J.-Y.; Wang, Y.; Huo, L.-H.; Cheng, X.-L.; Xu, Y.-M. Recent advances of emerging tin disulfide for room temperature gas sensing. *Rare Met.* **2023**, *42*, 3897–3913. [CrossRef]
6. Chen, Y.; Li, Z.; Tang, T.; Cheng, Y.; Cheng, L.; Wang, X.; Haidry, A.A.; Jannat, A.; Ou, J.Z. Room-Temperature Optoelectronic NO_2 Sensing Using Two-Dimensional Gallium Oxyselenides. *ACS Appl. Nano Mater.* **2024**, *7*, 3229–3238. [CrossRef]
7. Cheng, X.; Yao, Y.; Zheng, S.; Wan, Y.; Wei, C.; Yang, G.; Yuan, Y.; Tsai, H.-S.; Wang, Y.; Hao, J. Te@Se Core–Shell Heterostructures with Tunable Shell Thickness for Ultra-Stable NO_2 Detection. *ACS Sens.* **2025**, *10*, 283–291. [CrossRef]
8. Tang, T.; Li, Z.; Liu, Y.Y.; Chen, Y.L.; Cheng, Y.F.; Liang, Y.; Zhuang, J.H.; Hu, X.Y.; Jannat, A.; Ou, R.; et al. Ultrathin two-dimensional titanium oxysulfide for enhanced sensitivity and stability of room temperature NO_2 sensing. *Ceram. Int.* **2025**, *51*, 3216–3223. [CrossRef]
9. Huang, H.; Pan, Z.; Wang, J.; Wang, T.; Yang, W.; Yu, H.; Li, F.; Dong, X.; Yang, Y. Ag nanoparticles sensitized ZnO/MoS_2 composites to detect ppb-level NO_2 and automobile exhaust gas. *Sens. Actuators B Chem.* **2025**, *433*, 137569. [CrossRef]
10. Yu, M.; Li, J.; Yin, D.; Zhou, Z.; Wei, C.; Wang, Y.; Hao, J. Enhanced oxygen anions generation on Bi_2S_3/Sb_2S_3 heterostructure by visible light for trace H_2S detection at room temperature. *J. Hazard. Mater.* **2024**, *476*, 134932. [CrossRef]
11. Huang, H.; Zhao, J.; Pan, Z.; Wang, T.; Yu, H.; Li, F.; Dong, X.; Liu, Z.; Yang, Y. rGO doped MOFs-derived CuO nanocomposites as flexible room-temperature sensors for ppb-level H_2S detection. *Sens. Actuators B Chem.* **2025**, *422*, 136596. [CrossRef]
12. Shen, S.-K.; Xin, Y.-Y.; Zhang, X.-F.; Zhou, X.; Deng, Z.-P.; Xu, Y.-M.; Huo, L.-H.; Gao, S. Corn stigma template-assisted synthesis of single crystal MoO_3 elliptical nanosheets for chemiresistive detection of dibutylamine vapor. *Sens. Actuators B Chem.* **2024**, *408*, 135480. [CrossRef]
13. Li, J.; Zheng, M.; Yang, M.; Zhang, X.; Cheng, X.; Zhou, X.; Gao, S.; Xu, Y.; Huo, L. Three-in-one Ni doped porous SnO_2 nanorods sensor: Controllable oxygen vacancies content, surface site activation and low power consumption for highly selective NO_2 monitoring. *Sens. Actuators B Chem.* **2023**, *382*, 133550. [CrossRef]
14. Gai, L.-Y.; Lai, R.-P.; Dong, X.-H.; Wu, X.; Luan, Q.-T.; Wang, J.; Lin, H.-F.; Ding, W.-H.; Wu, G.-L.; Xie, W.-F. Recent advances in ethanol gas sensors based on metal oxide semiconductor heterojunctions. *Rare Met.* **2022**, *41*, 1818–1842. [CrossRef]
15. Sun, X.; Gao, R.; Wu, Y.; Zhang, X.; Cheng, X.; Gao, S.; Xu, Y.; Huo, L. Novel in-situ deposited V_2O_5 nanorods array film sensor with enhanced gas sensing performance to n-butylamine. *Chem. Eng. J.* **2023**, *459*, 141505. [CrossRef]
16. Goswami, P.; Gupta, G. Recent progress of flexible NO_2 and NH_3 gas sensors based on transition metal dichalcogenides for room temperature sensing. *Mater. Today Chem.* **2022**, *23*, 100726. [CrossRef]
17. Zhang, L.; Khan, K.; Zou, J.; Zhang, H.; Li, Y. Recent Advances in Emerging 2D Material-Based Gas Sensors: Potential in Disease Diagnosis. *Adv. Mater. Interfaces* **2019**, *6*, 1901329. [CrossRef]
18. Milone, A.; Monteduro, A.G.; Rizzato, S.; Leo, A.; Di Natale, C.; Kim, S.S.; Maruccio, G. Advances in Materials and Technologies for Gas Sensing from Environmental and Food Monitoring to Breath Analysis. *Adv. Sustain. Syst.* **2022**, *7*, 2200083. [CrossRef]
19. Rosolina, S.M.; Carpenter, T.S.; Xue, Z.-L. Bismuth-Based, Disposable Sensor for the Detection of Hydrogen Sulfide Gas. *Anal. Chem.* **2016**, *88*, 1553–1558. [CrossRef]
20. Potyrailo, R.A. Multivariable Sensors for Ubiquitous Monitoring of Gases in the Era of Internet of Things and Industrial Internet. *Chem. Rev.* **2016**, *116*, 11877–11923. [CrossRef]
21. Jeong, S.Y.; Kim, J.S.; Lee, J.H. Rational Design of Semiconductor-Based Chemiresistors and their Libraries for Next-Generation Artificial Olfaction. *Adv. Mater.* **2020**, *32*, 2002075. [CrossRef]
22. Ji, H.; Zeng, W.; Li, Y. Gas sensing mechanisms of metal oxide semiconductors: A focus review. *Nanoscale* **2019**, *11*, 22664–22684. [CrossRef] [PubMed]
23. Yu, H.; Guo, C.; Zhang, X.; Xu, Y.; Cheng, X.; Gao, S.; Huo, L. Recent Development of Hierarchical Metal Oxides Based Gas Sensors: From Gas Sensing Performance to Applications. *Adv. Sustain. Syst.* **2022**, *6*, 2100370. [CrossRef]

24. Wu, R.; Hao, J.; Wang, Y. Recent Advances in Engineering of 2D Layered Metal Chalcogenides for Resistive-Type Gas Sensor. *Small* **2024**, *20*, 2404821. [CrossRef]
25. Cui, S.; Pu, H.; Wells, S.A.; Wen, Z.; Mao, S.; Chang, J.; Hersam, M.C.; Chen, J. Ultrahigh sensitivity and layer-dependent sensing performance of phosphorene-based gas sensors. *Nat. Commun.* **2015**, *6*, 8632. [CrossRef] [PubMed]
26. Zhao, Q.-N.; Zhang, Y.-J.; Duan, Z.-H.; Wang, S.; Liu, C.; Jiang, Y.-D.; Tai, H.-L. A review on $Ti_3C_2T_x$-based nanomaterials: Synthesis and applications in gas and humidity sensors. *Rare Met.* **2020**, *40*, 1459–1476. [CrossRef]
27. Qiu, L.; Huo, Y.; Pan, Z.; Wang, T.; Yu, H.; Liu, X.; Tong, X.; Yang, Y. Resister-type sensors based on $Ti_3C_2T_x$ MXene decorated In_2O_3 p-n heterojunction for ppb-level NO_2 detection at room temperature. *J. Environ. Chem. Eng.* **2025**, *13*, 115249. [CrossRef]
28. Sang, D.K.; Wang, H.; Guo, Z.; Xie, N.; Zhang, H. Recent Developments in Stability and Passivation Techniques of Phosphorene toward Next-Generation Device Applications. *Adv. Funct. Mater.* **2019**, *29*, 1903419. [CrossRef]
29. Lee, E.; Yoon, Y.S.; Kim, D.-J. Two-Dimensional Transition Metal Dichalcogenides and Metal Oxide Hybrids for Gas Sensing. *ACS Sens.* **2018**, *3*, 2045–2060. [CrossRef]
30. Li, J.; Zhang, Y.; Huo, M.; Ho, S.-H.; Tsai, H.-S. Metallic group VB transition metal dichalcogenides for electrochemical energy storage. *Mater. Today Chem.* **2022**, *26*, 101241. [CrossRef]
31. Choi, W.; Choudhary, N.; Han, G.H.; Park, J.; Akinwande, D.; Lee, Y.H. Recent development of two-dimensional transition metal dichalcogenides and their applications. *Mater. Today* **2017**, *20*, 116–130. [CrossRef]
32. Agrawal, A.V.; Kumar, N.; Kumar, M. Strategy and Future Prospects to Develop Room-Temperature-Recoverable NO_2 Gas Sensor Based on Two-Dimensional Molybdenum Disulfide. *Nano-Micro Lett.* **2021**, *13*, 38. [CrossRef] [PubMed]
33. Zhang, H.; Zhang, Z.; Zhan, Q.; Liu, D.; Zhao, P.; Cheng, Y. Recent advances of substitutionally doped tin dichalcogenides. *J. Mater. Chem. C* **2022**, *10*, 7771–7782. [CrossRef]
34. Tang, H.; Sacco, L.N.; Vollebregt, S.; Ye, H.; Fan, X.; Zhang, G. Recent advances in 2D/nanostructured metal sulfide-based gas sensors: Mechanisms, applications, and perspectives. *J. Mater. Chem. A* **2020**, *8*, 24943–24976. [CrossRef]
35. Hermawan, A.; Septiani, N.L.W.; Taufik, A.; Yuliarto, B.; Suyatman; Yin, S. Advanced Strategies to Improve Performances of Molybdenum-Based Gas Sensors. *Nano-Micro Lett.* **2021**, *13*, 207. [CrossRef]
36. Guo, X.; Zhang, F.; Zhang, Y.; Hu, J. Review on the advancement of SnS_2 in photocatalysis. *J. Mater. Chem. A* **2023**, *11*, 7331–7343. [CrossRef]
37. Ansari, M.Z.; Ansari, S.A.; Kim, S.-H. Fundamentals and recent progress of Sn-based electrode materials for supercapacitors: A comprehensive review. *J. Energy Storage* **2022**, *53*, 105187. [CrossRef]
38. Guo, Y.; Ao, Y.; Wang, P.; Wang, C. Mediator-free direct dual-Z-scheme $Bi_2S_3/BiVO_4/MgIn_2S_4$ composite photocatalysts with enhanced visible-light-driven performance towards carbamazepine degradation. *Appl. Catal. B Environ.* **2019**, *254*, 479–490. [CrossRef]
39. Dong, Y.; Hu, M.; Zhang, Z.; Zapien, J.A.; Wang, X.; Lee, J.-M. Hierarchical self-assembled $Bi2S_3$ hollow nanotubes coated with sulfur-doped amorphous carbon as advanced anode materials for lithium ion batteries. *Nanoscale* **2018**, *10*, 13343–13350. [CrossRef]
40. Liu, L.; Gao, Y.; Hu, Q. Controllable Epitaxial-like Growth of Bi_2S_3/MoS_2 Hybrid Aerogel Nanostructures for Sensitive NO_2 Detection at Room Temperature. *ACS Appl. Nano Mater.* **2023**, *6*, 8260–8269. [CrossRef]
41. Wang, T.; Liu, J.; Zhang, Y.; Liang, Q.; Wu, R.; Tsai, H.-S.; Wang, Y.; Hao, J. Bifunctional gas sensor based on Bi_2S_3/SnS_2 heterostructures with improved selectivity through visible light modulation. *J. Mater. Chem. A* **2022**, *10*, 4306–4315. [CrossRef]
42. Afsar, M.F.; Rafiq, M.A.; Jamil, A.; Fareed, S.; Siddique, F.; Tok, A.I.Y.; Hasan, M.M.U. Development of High-Performance Bismuth Sulfide Nanobelts Humidity Sensor and Effect of Humid Environment on its Transport Properties. *ACS Omega* **2019**, *4*, 2030–2039. [CrossRef]
43. Ali, S.; Kazmi, S.M.T.; Sher, F.; Nigah, A.; Bilal, M.; Rafiq, M.A. Fast, Sensitive, and Selective Hydrogen Sensing of Silver-Doped Bismuth Sulfide Nanobelts. *J. Electron. Mater.* **2024**, *53*, 2753–2762. [CrossRef]
44. Fang, L.; Qiu, Y.; Zhai, T.; Wang, F.; Lan, M.; Huang, K.; Jing, Q. Flower-like nanoarchitecture assembled from Bi_2S_3 nanorod/MoS_2 nanosheet heterostructures for high-performance supercapacitor electrodes. *Colloids Surf. A Physicochem. Eng. Asp.* **2017**, *535*, 41–48. [CrossRef]
45. Furukawa, R.; Hasegawa, T.; Okawa, A.; Yin, S. One-pot facile synthesis of rod-like Bi_2S_3 particles in deep eutectic solvent and their ppb-level selective H_2S gas detection. *Dalton Trans.* **2024**, *53*, 18116–18121. [CrossRef] [PubMed]
46. Guo, C.F.; Cao, S.; Zhang, J.; Tang, H.; Guo, S.; Tian, Y.; Liu, Q. Topotactic Transformations of Superstructures: From Thin Films to Two-Dimensional Networks to Nested Two-Dimensional Networks. *J. Am. Chem. Soc.* **2011**, *133*, 8211–8215. [CrossRef]
47. Dhar, N.; Syed, N.; Mohiuddin, M.; Jannat, A.; Zavabeti, A.; Zhang, B.Y.; Datta, R.S.; Atkin, P.; Mahmood, N.; Esrafilzadeh, D.; et al. Exfoliation Behavior of van der Waals Strings: Case Study of Bi_2S_3. *ACS Appl. Mater. Interfaces* **2018**, *10*, 42603–42611. [CrossRef]

48. Messalea, K.A.; Zavabeti, A.; Mohiuddin, M.; Syed, N.; Jannat, A.; Atkin, P.; Ahmed, T.; Walia, S.; McConville, C.F.; Kalantar-Zadeh, K.; et al. Two-Step Synthesis of Large-Area 2D Bi_2S_3 Nanosheets Featuring High In-Plane Anisotropy. *Adv. Mater. Interfaces* **2020**, *7*, 2001131. [CrossRef]
49. Yao, K.; Gong, W.W.; Hu, Y.F.; Liang, X.L.; Chen, Q.; Peng, L.M. Individual Bi_2S_3 Nanowire-Based Room-Temperature H_2 Sensor. *J. Phys. Chem. C* **2008**, *112*, 4.
50. Yang, X.; Tian, S.; Li, R.; Wang, W.; Zhou, S. Use of single-crystalline Bi_2S_3 nanowires as room temperature ethanol sensor synthesized by hydrothermal approach. *Sens. Actuators B Chem.* **2017**, *241*, 210–216. [CrossRef]
51. Kan, H.; Li, M.; Song, Z.; Liu, S.; Zhang, B.; Liu, J.; Li, M.-Y.; Zhang, G.; Jiang, S.; Liu, H. Highly sensitive response of solution-processed bismuth sulfide nanobelts for room-temperature nitrogen dioxide detection. *J. Colloid Interface Sci.* **2017**, *506*, 102–110. [CrossRef] [PubMed]
52. Feng, Q.; Xie, X.; Zhang, M.; Liao, N. First-principles investigation of Bi_2S_3 as sensitive and selective NO_2 sensor upon humidity exposure. *J. Mater. Sci.* **2023**, *58*, 2198–2208. [CrossRef]
53. Luo, J.; Feng, X.; Kan, H.; Li, H.; Fu, C. One-Dimensional Bi_2S_3 Nanobelts-Based Surface Acoustic Wave Sensor for NO_2 Detection at Room Temperature. *IEEE Sens. J.* **2021**, *21*, 1404–1408. [CrossRef]
54. Yang, Y.; Zhu, M.; Zhang, H.; Wang, B.; Chen, C.; Li, J.; Wang, Y.; Hao, J. Room temperature gas sensor based on rGO/Bi_2S_3 heterostructures for ultrasensitive and rapid NO_2 detection. *Chem. Eng. J.* **2024**, *490*, 151872. [CrossRef]
55. Kan, H.; Yang, W.; Guo, Z.; Li, M. Highly sensitive room-temperture NO_2 gas sensor based on Bi_2S_3 nanorods. *J. Mater. Sci. Mater. Electron.* **2024**, *35*, 331. [CrossRef]
56. Yang, Y.; Liu, C.; Wang, Y.; Hao, J. Nanorods Assembled Hierarchical Bi_2S_3 for Highly Sensitive Detection of Trace NO_2 at Room Temperature. *Chemosensors* **2024**, *12*, 8. [CrossRef]
57. Cheng, Y.; Chang, Y.; Feng, Y.; Jian, H.; Tang, Z.; Zhang, H. Deep-Level Defect Enhanced Photothermal Performance of Bismuth Sulfide–Gold Heterojunction Nanorods for Photothermal Therapy of Cancer Guided by Computed Tomography Imaging. *Angew. Chem. Int. Ed.* **2017**, *57*, 246–251. [CrossRef]
58. Zhou, T.; Zhang, T. Recent Progress of Nanostructured Sensing Materials from 0D to 3D: Overview of Structure–Property-Application Relationship for Gas Sensors. *Small Methods* **2021**, *5*, 2100515. [CrossRef]
59. Chen, Z.; Cao, M. Synthesis, characterization, and hydrophobic properties of Bi_2S_3 hierarchical nanostructures. *Mater. Res. Bull.* **2011**, *46*, 555–562. [CrossRef]
60. Jia, T.; Wang, X.; Long, F.; Li, J.; Kang, Z.; Fu, F.; Sun, G.; Chen, J. Facile Synthesis, Characterization, and Visible-light Photocatalytic Activities of 3D Hierarchical Bi_2S_3 Architectures Assembled by Nanoplatelets. *Crystals* **2016**, *6*, 140. [CrossRef]
61. Fu, T.-X. Gas sensor based on three dimensional Bi_2S_3 nanowires network for ammonia detection at room temperature. *Mater. Res. Bull.* **2018**, *99*, 460–465. [CrossRef]
62. Li, H.; Yang, J.; Zhang, J.; Zhou, M. Facile synthesis of hierarchical Bi_2S_3 nanostructures for photodetector and gas sensor. *RSC Adv.* **2012**, *2*, 6258–6261. [CrossRef]
63. Yang, Y.; Xin, T.; Liu, C.; Zhang, T.; Hao, W.; Wang, Y.; Hao, J. Urchin-like Bi_2S_3 nanostructures with rich sulfur vacancies for ppb-level NO_2 sensing. *J. Alloys Compd.* **2023**, *930*, 167467. [CrossRef]
64. Shen, G.; Chen, D.; Tang, K.; Li, F.; Qian, Y. Large-scale synthesis of uniform urchin-like patterns of Bi_2S_3 nanorods through a rapid polyol process. *Chem. Phys. Lett.* **2003**, *370*, 334–337. [CrossRef]
65. Lu, J.; Han, Q.; Yang, X.; Lu, L.; Wang, X. Microwave-assisted synthesis and characterization of 3D flower-like Bi_2S_3 superstructures. *Mater. Lett.* **2007**, *61*, 2883–2886. [CrossRef]
66. Tang, J.; Alivisatos, A.P. Crystal Splitting in the Growth of Bi_2S_3. *Nano Lett.* **2006**, *6*, 2701–2706. [PubMed]
67. Han, D.; Du, M.-H.; Dai, C.-M.; Sun, D.; Chen, S. Influence of defects and dopants on the photovoltaic performance of Bi_2S_3: First-principles insights. *J. Mater. Chem. A* **2017**, *5*, 6200–6210. [CrossRef]
68. Sun, H.; Jiang, Z.; Wu, D.; Ye, L.; Wang, T.; Wang, B.; An, T.; Wong, P.K. Defect-Type-Dependent Near-Infrared-Driven Photocatalytic Bacterial Inactivation by Defective Bi_2S_3 nanorods. *ChemSusChem* **2019**, *12*, 890–897. [CrossRef] [PubMed]
69. Chen, X.; Shi, J.; Wang, T.; Zheng, S.; Lv, W.; Chen, X.; Yang, J.; Zeng, M.; Hu, N.; Su, Y.; et al. High-Performance Wearable Sensor Inspired by the Neuron Conduction Mechanism through Gold-Induced Sulfur Vacancies. *ACS Sens.* **2022**, *7*, 816–826. [CrossRef] [PubMed]
70. Bag, A.; Lee, N.-E. Gas sensing with heterostructures based on two-dimensional nanostructured materials: A review. *J. Mater. Chem. C* **2019**, *7*, 13367–13383. [CrossRef]
71. Ma, S.; Yang, D.; Li, B.; Guan, Y.; Wu, M.; Wu, J.; Guo, Y.; Sheng, L.; Liu, L.; Yao, T. An interfacial C-S bond bridged S-scheme ZnS/C_3N_5 for photocatalytic H_2 evolution: Opposite internal-electric-field of ZnS/C_3N_4, increased field strength, and accelerated surface reaction. *J. Colloid Interface Sci.* **2024**, *664*, 960–971. [CrossRef]
72. Ghuge, R.S.; Shinde, M.D.; Rane, S.B. Bismuth-Based Gas Sensors: A Comprehensive Review. *J. Electron. Mater.* **2021**, *50*, 6060–6072. [CrossRef]

73. Chen, X.; Wang, T.; Shi, J.; Lv, W.; Han, Y.; Zeng, M.; Yang, J.; Hu, N.; Su, Y.; Wei, H.; et al. A Novel Artificial Neuron-Like Gas Sensor Constructed from CuS Quantum Dots/Bi_2S_3 Nanosheets. *Nano-Micro Lett.* **2021**, *14*, 8. [CrossRef]
74. Pei, Y.; Li, X.; Chu, H.; Ge, Y.; Dong, P.; Baines, R.; Pei, L.; Ye, M.; Shen, J. Anion-exchange engineering of cookie-like Bi_2S_3/Bi_2MoO_6 heterostructure for enhanced photocatalytic activities and gas-sensing properties. *Talanta* **2017**, *165*, 44–51. [CrossRef] [PubMed]
75. Zhao, X.; Zhi, M.; Hang, D.; Ren, Q.; Zhang, P.; Chen, C.; Chen, Q.; Li, Q.; Zhang, Z.; Yan, J.; et al. Ultrasensitive NO_2 gas sensor based on MoS_2 modified urchin-like Bi_2S_3 heterojunction. *Phys. E Low-Dimens. Syst. Nanostruct.* **2023**, *147*, 115575. [CrossRef]
76. Zhao, Z.; Su, Z.; Lv, Z.; Shi, P.; Jin, G.; Wu, L. Room temperature gas sensors for NH_3 detection based on the heterojunction of 2D $Ti_3C_2T_x$ MXenes and Bi_2S_3. *Microchim. Acta* **2024**, *191*, 687. [CrossRef]
77. Hao, J.; Zhang, D.; Sun, Q.; Zheng, S.; Sun, J.; Wang, Y. Hierarchical SnS_2/SnO_2 nanoheterojunctions with increased active-sites and charge transfer for ultrasensitive NO_2 detection. *Nanoscale* **2018**, *10*, 7210–7217. [CrossRef] [PubMed]
78. Yang, Y.; Mao, J.; Yin, D.; Zhang, T.; Liu, C.; Hao, W.; Wang, Y.; Hao, J. Synergy of S-vacancy and heterostructure in BiOCl/Bi_2S_{3-x} boosting room-temperature NO_2 sensing. *J. Hazard. Mater.* **2023**, *455*, 131591. [CrossRef]
79. Hu, C.; Yu, M.; Zhou, Z.; Wei, C.; Wang, Y.; Hao, J. Rapid room-temperature H_2S detection based on Bi_2S_3/CuO heterostructures: The synergy of increased surface-adsorbed oxygen and a heterojunction effect. *Inorg. Chem. Front.* **2025**, *12*, 578–587. [CrossRef]
80. Cheng, Y.; Ren, B.; Xu, K.; Jeerapan, I.; Chen, H.; Li, Z.; Ou, J.Z. Recent progress in intrinsic and stimulated room-temperature gas sensors enabled by low-dimensional materials. *J. Mater. Chem. C* **2021**, *9*, 3026–3051. [CrossRef]
81. Lim, K.; Jo, Y.M.; Yoon, J.W.; Kim, J.S.; Lee, D.J.; Moon, Y.K.; Yoon, J.W.; Kim, J.H.; Choi, H.J.; Lee, J.H. A Transparent Nanopatterned Chemiresistor: Visible-Light Plasmonic Sensor for Trace-Level NO_2 Detection at Room Temperature. *Small* **2021**, *17*, 2100438. [CrossRef] [PubMed]
82. Suh, J.M.; Eom, T.H.; Cho, S.H.; Kim, T.; Jang, H.W. Light-activated gas sensing: A perspective of integration with micro-LEDs and plasmonic nanoparticles. *Mater. Adv.* **2021**, *2*, 827–844. [CrossRef]
83. Liu, D.; Tang, Z.; Zhang, Z. Comparative study on NO_2 and H_2S sensing mechanisms of gas sensors based on WS_2 nanosheets. *Sens. Actuators B Chem.* **2020**, *303*, 127114. [CrossRef]
84. Liu, J.; Xin, T.; Yang, Z.; Hao, W.; Wang, Y.; Hao, J. Bi_2S_3/ZnS heterostructures for H_2S sensing in the dark: The synergy of increased surface-adsorbed oxygen and charge transfer. *Inorg. Chem. Front.* **2022**, *9*, 4921–4929. [CrossRef]
85. Li, X.; Quan, W.; Yang, R.; Li, X.; Wu, J.; Fan, C.; Lv, W.; Liu, X.; Zeng, M.; Yang, J.; et al. Bismuth Sulfide Nanorod/Vanadium Carbide MXene as Nitrogen Dioxide Gas Sensor Operating at Room Temperature under Ultraviolet-Assisted Recovery. *ACS Appl. Nano Mater.* **2024**, *7*, 23882–23893. [CrossRef]

Disclaimer/Publisher's Note: The statements, opinions and data contained in all publications are solely those of the individual author(s) and contributor(s) and not of MDPI and/or the editor(s). MDPI and/or the editor(s) disclaim responsibility for any injury to people or property resulting from any ideas, methods, instructions or products referred to in the content.